Radiation-induced defects and their recombination processes in the x-ray storage phosphor $BaBr_2:Eu^{2+}$

2003 J. Phys.: Condens. Matter 15 2061

(http://iopscience.iop.org/0953-8984/15/12/323)

INSTITUTE OF PHYSICS PUBLISHING JOURNAL OF PHYSICS: CONDENSED MATTER

J. Phys.: Condens. Matter **15** (2003) 2061–2070 PII: S0953-8984(03)57856-0

Radiation-induced defects and their recombination processes in the x-ray storage phosphor $BaBr_2:Eu^{2+}$

M Secu, S Schweizer[1], U Rogulis[2] and J-M Spaeth

Universität Paderborn, Department Physik, Warburger Straße 100, D-33098 Paderborn, Germany

E-mail: schweizer@physik.upb.de

Received 6 January 2003
Published 17 March 2003
Online at stacks.iop.org/JPhysCM/15/2061

Abstract

The recombination processes in the x-ray storage phosphor $BaBr_2:Eu^{2+}$ were investigated by optical and magneto-optical methods. A structure-sensitive investigation of the defects involved in the recombination processes was performed by detecting the microwave-induced changes in the recombination luminescence in a high magnetic field. F centres as well as V_K hole centres are created after x-irradiation at low temperatures. The low-energy recombination band peaking at about 460 nm is due to F–V_K centre recombinations, whereas the two high energy bands at 282 and 315 nm are probably due to recombinations of self-trapped excitons.

1. Introduction

X-ray storage phosphors are materials which can store an x-ray-induced latent image in the form of electron and hole trap centres. The stored information is recovered by optical stimulation of the electron trap centres with visible light. Upon photostimulation, their electrons recombine with the hole centres resulting in a luminescence at a nearby activator doped in addition, which is usually a rare-earth ion. This process is called photostimulated luminescence (PSL). Promising candidates as x-ray storage phosphors of this kind which promise high spatial resolution are the activator-doped fluorozirconate glasses, in which PSL-active $BaBr_2$ nanoparticles were found [1]. It was proposed that the PSL of the Eu^{2+}-doped fluorobromozirconate glass is due to the small $BaBr_2$:Eu crystalline precipitates, which were found in the hexagonal or in the orthorhombic phase depending on the procedure of annealing of the Br^--doped glass [2]. Both glass ceramics show a recombination afterglow after switching off the x-ray radiation [3]. For the understanding of the glass ceramic x-ray storage phosphors it is essential to investigate the storage and read-out processes of bulk $BaBr_2$ as a basis for the detailed investigation of the glass ceramics.

[1] Author to whom any correspondence should be addressed.
[2] Permanent address: Institute of Solid State Physics, University of Latvia, LV-1063 Riga, Latvia.

0953-8984/03/122061+10$30.00

After switching off the x-ray excitation, orthorhombic $BaBr_2$ shows an intense recombination afterglow at room temperature which is even more intense at low temperatures. After additive or electrolytic coloration or after x-irradiation of $BaBr_2$ at low temperatures, F centres (electrons trapped in halide vacancies) [4–6] and self-trapped hole centres (V_K centres—holes shared between two adjacent halide ions) [7, 8] could be created. The aim of this paper is the investigation of the radiation-induced defects and their recombination processes in orthorhombic $BaBr_2$ by means of optical and magneto-optical methods. The detection of the microwave-induced changes in the recombination luminescence (RL) in a high field allows a structure-sensitive investigation of the participating defects. This method has already been successfully applied for the investigation of the recombination processes in the x-ray storage phosphor $BaFBr:Eu^{2+}$ [9, 10]. Magnetic circular dichroism methods would have been ineffective due to the optical anisotropy of $BaBr_2$. The participation of F centres, V_K centres, as well as Eu^{2+} in europium-doped $BaBr_2$ will be discussed.

2. Experiment

2.1. Sample preparation

Single crystals of orthorhombic $BaBr_2$ were grown in the Paderborn crystal growth laboratory using the Bridgman method with a quartz glass ampoule, $SiBr_4$ atmosphere, and $BaBr_2$ powder. For the europium- or oxygen-doped samples, 1000 ppm of $EuBr_2$ or 100 ppm of BaO, respectively, were added. The usual technique was modified for careful annealing and slow cooling through the cubic–orthorhombic phase transformation near 800 °C [11]. Prior to crystal growth the $BaBr_2$ powder was dried in vacuum with subsequent melting in a $SiBr_4$ atmosphere to reduce the oxygen contamination. The $BaBr_2$ single crystals were oriented using Laue techniques and cut to obtain samples with dimensions of a few millimetres along the main crystallographic directions.

2.2. Spectroscopy

2.2.1. Luminescence and absorption. X-ray luminescence (XL) and RL spectra were measured with a single-beam spectrometer in which a 0.25 m double monochromator (Spex) was used for the luminescence. The XL signal was recorded under x-ray excitation with a stationary x-ray tube (tungsten anode, 50 kV, 30 mA); a RL signal could be observed after switching off the x-ray excitation. The luminescence was detected in the spectral range of 250–600 nm using single-photon counting with a cooled photomultiplier. Optical absorption spectra were recorded in the visible spectral range from 380 to 800 nm also using a 0.25 m double monochromator (Spex). The luminescence spectra were not corrected for the spectral sensitivity of the experimental set-up. For low-temperature measurements a continuous flow helium cryostat was used.

Thermostimulated luminescence (TSL) curves were recorded in the temperature range from 15 to 150 K using a heating rate of 0.05 K s^{-1}. Prior to the optical absorption and TSL measurements the samples were x-irradiated at 15 K (tungsten anode, 50 kV, 30 mA).

2.2.2. Recombination luminescence-detected electron paramagnetic resonance. Recombination luminescence-detected electron paramagnetic resonance (RL-EPR) spectra were recorded with a custom-built, computer-controlled spectrometer working at 25 GHz (K band) or at 93 GHz (W band), respectively. All RL-EPR spectra were detected in the afterglow luminescence at 1.5 K using a cooled photomultiplier operating in the spectral range of 200–800 nm.

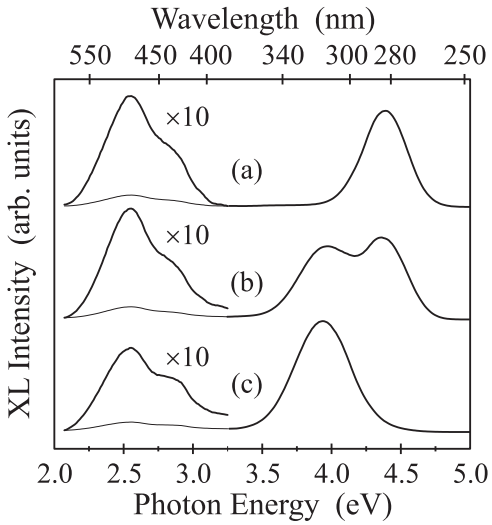

Figure 1. The temperature dependence of the XL of single-crystalline $BaBr_2$, recorded at (a) 15 K, (b) 37 K, and (c) 85 K. All spectra are normalized and partially scaled up by a factor of 10.

Prior to the measurements the samples were x-irradiated at 4.2 K with a mobile x-ray tube (tungsten anode, 60 kV, 15 mA, 20 min). Immediately after the x-ray excitation the RL-EPR was recorded either in the integral RL or in different spectral ranges using edge filters. In all RL-EPR spectra the magnetic field-dependent background was subtracted.

3. Experimental results

3.1. X-ray luminescence and thermostimulated luminescence

Figure 1 shows the XL spectra of $BaBr_2$, recorded at different temperatures. At 15 K, there is a strong peak at 282 nm (4.41 eV) and two less intense ones at 430 nm (2.88 eV) and 490 nm (2.55 eV) (see figure 1(a)). The 282 nm peak starts to disappear above about 40 K and a new band at 315 nm (3.95 eV) shows up (figure 1(b)). The XL spectrum, recorded at 85 K, shows only the peak at 315 nm (figure 1(c)). The spectra are partially scaled up by a factor of 10. The original spectra are indicated as thin solid curves. The 315 nm band disappears at about 150 K. At room temperature only the weak 430 and 490 nm bands could be observed.

The glow curve, recorded in the integral luminescence from 200 to 800 nm after x-irradiation at 15 K, shows two peaks at 31 and 106 K (figure 2). The activation energies for these two peaks computed by applying the best-fit method are (0.050 ± 0.005) and (0.27 ± 0.02) eV, respectively. The peak shape method yields the same results [12]. The TSL spectra depicted in figure 3 (curves (a) and (b)) show the 282 and the 390–550 nm bands for the 31 K peak and predominantly the 390–550 nm band for the 106 K peak. The TSL spectra agree with the XL spectra in the spectral position of the observed bands, but not in the relative intensity ratio between the 282 nm (315 nm) and the 390–550 nm band.

Figure 4 shows the optical absorption spectra, recorded immediately after x-irradiation and after subsequent annealing steps to 40 and 135 K, respectively. The spectra were recorded at 15 K. After x-irradiation a broad band peaking at about 490 nm, which is very close to the V_K centre absorption band at 460 nm (2.70 eV) found for x-irradiated $BaBr_2$:K [8], could be observed (figure 4, solid curve). The two additional peaks at 595 nm (2.08 eV) and 735 nm

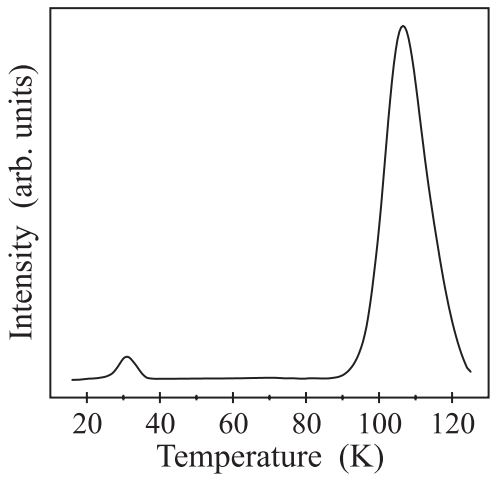

Figure 2. The glow curve of $BaBr_2$ after x-irradiation at 15 K. The irradiation time was 15 min.

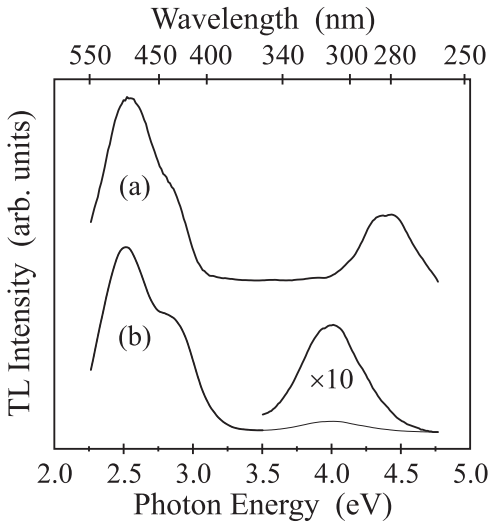

Figure 3. TSL spectra of single-crystalline $BaBr_2$, recorded at (a) 31 K and (b) 107 K. Prior to the measurement the sample was x-irradiated at 15 K for 15 min. All spectra are normalized.

(1.69 eV) can be assigned to F centre absorption bands [4–6]. Within experimental error no change could be observed after subsequent annealing to 40 K (figure 4, dashed curve). However, after annealing to 135 K a significant decrease of the F centre absorption bands as well as of the V_K band could be observed (figure 4, dotted curve).

The XL of oxygen-doped $BaBr_2$ (figure 5(b), solid curve) is identical to that of undoped $BaBr_2$ (figure 5(a), solid curve). For the Eu-doped $BaBr_2$ a very intense peak at 403 nm (3.08 eV) and the 490 nm band could be observed (figure 5(c), solid curve). The 430 nm band is probably hidden under the intense 403 nm band. The 403 nm band can be attributed to the 5d–4f transition of Eu^{2+} in $BaBr_2$ [13]. The spectral positions of the RL spectra (figure 5, dashed curves), recorded at 15 K after switching off the x-ray excitation, agree fairly well with the XL spectra described above. The RL intensity is significantly lower after x-irradiation

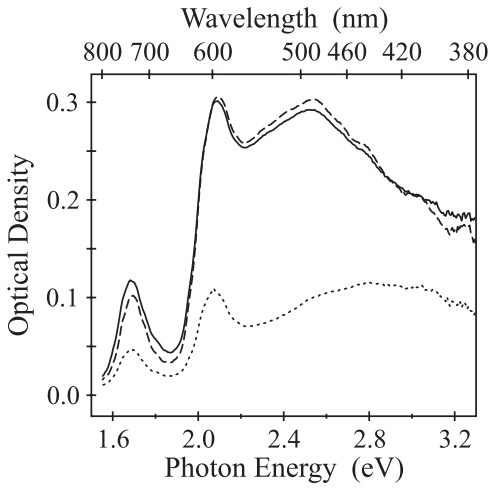

Figure 4. Absorption spectra of $BaBr_2$, recorded directly after x-irradiation at 15 K (solid curve), after subsequent annealing to 40 K (dashed curve), and after annealing to 135 K (dotted curve). The optical densities represent the differences between the optical densities before and after x-irradiation and subsequent annealing steps. The irradiation time was 60 min.

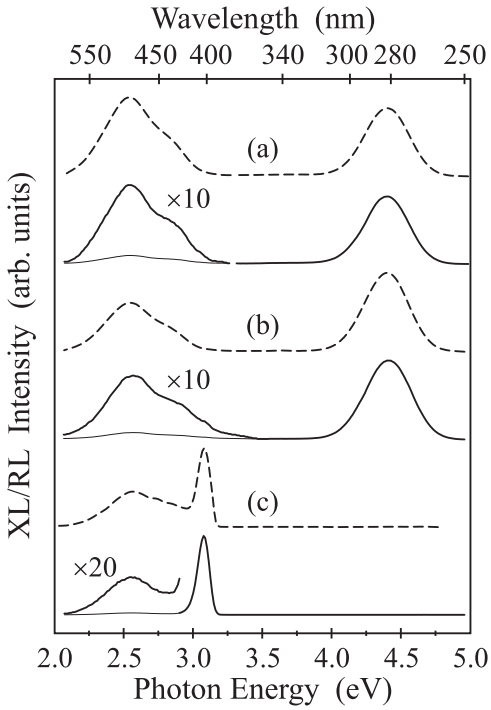

Figure 5. X-ray (solid curve) and recombination (dashed curve) luminescence spectra of (a) $BaBr_2$, (b) $BaBr_2$:BaO, and (c) $BaBr_2:Eu^{2+}$, recorded at 15 K under (XL) or after (RL) x-irradiation. All spectra are normalized. The XL spectra are partially scaled up.

above about 125 K. After x-irradiation at room temperature the RL could hardly be detected. All RL bands described above could also be observed upon additional photostimulation in the F centre absorption bands.

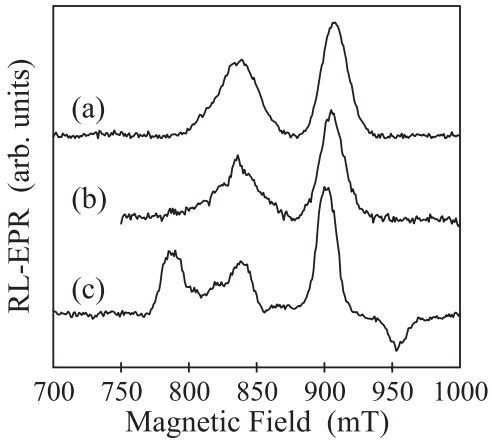

Figure 6. RL-EPR spectra of (a) $BaBr_2$ for $\vec{B} \parallel \vec{b}$, (b) BaB_2:BaO for $\vec{B} \parallel \vec{b}$, and (c) $BaBr_2$:Eu^{2+} for $\vec{B} \parallel \vec{c}$. All spectra were recorded at 1.5 K in the K band (25.15 GHz) after x-irradiation at 4.2 K. The RL was detected in the integral luminescence.

3.2. Recombination luminescence-detected electron paramagnetic resonance

The RL-EPR spectra of $BaBr_2$, oxygen-doped $BaBr_2$, and Eu-doped $BaBr_2$ are shown in figure 6. The spectra were recorded in the K band (25 GHz) at 1.5 K after x-irradiation at 4.2 K. The RL-EPR spectrum of $BaBr_2$ (figure 6(a)) shows two broad resonances at $g = 1.98$ (908 mT for 25.15 GHz) and $g = 2.15$ (836 mT for 25.15 GHz) which can be attributed to the F centre and the V_K centre, respectively, due to their g-factors and overall linewidths [4, 7]. The RL-EPR spectrum of oxygen-doped $BaBr_2$ (figure 6(b)) yields the same resonance lines as nominally pure $BaBr_2$; no additional resonances due to oxygen impurities could be observed. The V_K resonance line appears in the 460 nm RL band. In the 282 nm RL band no EPR lines could be detected. Figure 6(c) shows the RL-EPR spectrum of Eu-doped $BaBr_2$. Several broad resonance lines with changing sign could be observed. The lines could be assigned to the Eu^{2+} ground state because of the g-factor and the fine-structure splittings [15]. The F centre and the V_K centre lines are probably superimposed on the Eu^{2+} resonances and thus not resolved. As can already by seen from figure 5(c), the RL is mainly determined by the Eu^{2+} luminescence.

Figure 7 shows the angular dependence of the RL-EPR spectra of $BaBr_2$:Eu for a rotation of the magnetic field in the ac-plane. In contrast to the RL-EPR spectrum recorded in the K band, the W-band RL-EPR shows only the unresolved, structureless F centre resonance, but no Eu^{2+} lines. According to the $BaBr_2$ crystal structure [14] two different types of F centre, F_I and F_{II}, can be expected; both centres display C_S symmetry with a single-symmetry plane parallel to the ac-plane [6]. For each F centre type there are four different centre orientations (see figure 8). However, the EPR angular dependence of each F centre should contain only one structureless line for a rotation of the magnetic field in the ab- and bc-planes, but two lines for all other directions including all general directions in the ac-plane. The angular dependence was analysed using the spin Hamiltonian

$$\mathcal{H} = \mu_B \vec{B} \cdot \underline{\underline{g}} \cdot \vec{S} \tag{1}$$

where $\underline{\underline{g}}$ is the g-tensor, μ_B is the Bohr magneton, $\vec{B}$ is the magnetic field vector, and $\vec{S}$ is the electron spin operator. The principal axes system of the g-tensor can be obtained from the crystallographic system abc by a rotation around the b-axis, which is one of the principal

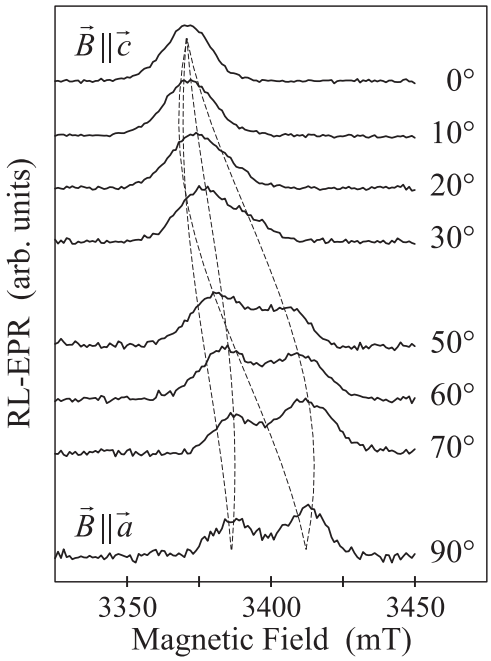

Figure 7. RL-EPR spectra of $BaBr_2$:Eu^{2+} for a rotation of the magnetic field in the *ca*-plane. All spectra were recorded at 1.5 K in the W band (93.7 GHz) after x-irradiation at 4.2 K. The RL was detected in the integral luminescence.

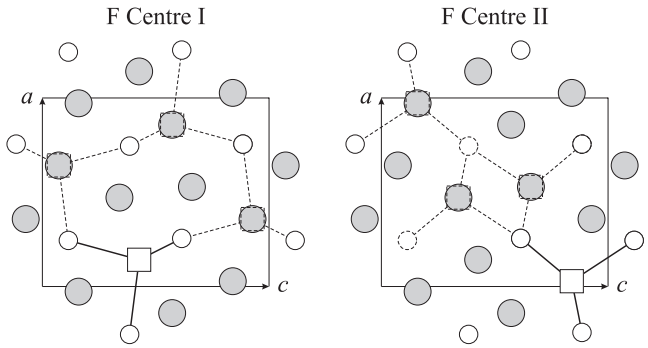

Figure 8. Projections of the two different F centres in the *ac*-symmetry plane of $BaBr_2$. Each F centre has four different centre orientations. The small white and large grey circles denote Ba^{2+} and Br^- ions, respectively. The ions distinguished by hatched circles lie in a different mirror plane to the non-hatched ones.

axes, the other two lying in the *ac*-type mirror plane. The parameters obtained are collected in table 1 and were used for the calculation of the dashed curves in figure 7. The assignment to F_I and F_{II} is arbitrary. The EPR data obtained do not allow a clear labelling of the two different F centres.

Table 1. Parameters of the spin Hamiltonian (equation (1)) for the two different F centres in $BaBr_2$. g_a, g_b, and g_c are the g-values for orientations of the magnetic field parallel to the crystallographic axes; ϑ describes the angle in the ac-mirror plane between the z-axis of the g-tensor and the c-axis of the crystal. The precision for g is ± 0.001.

Centre	g_a	g_b[a]	g_c	ϑ (deg)
F_I	1.976	—	1.986	<15
F_{II}	1.962	—	1.986	<15

[a] Not determined.

4. Discussion

In the K-band RL-EPR spectra of undoped and oxygen-doped $BaBr_2$, resonances of the F centre and the V_K centre could be observed. Detecting the RL with additional edge filters yielded the result that these resonances belong to the broad RL band at about 460 nm, i.e. this luminescence is due to F–V_K recombinations probably caused by tunnelling of close F–V_K pairs. This interpretation agrees with the strong decrease of these RL bands above 125 K where the V_K centres have almost gone. These luminescence bands could also be observed upon photostimulation in the F centre absorption bands. To explain this we assume that upon photostimulation, the electron from the F centre of distant and thus more stable F–V_K pairs could be re-trapped on a Br^- vacancy near to an isolated V_K centre leading to a close F–V_K pair which then recombines via tunnelling. Note, that the tunnelling probability is enhanced for a shorter distance between the recombining partners.

For Eu^{2+}-doped $BaBr_2$, resonances of the Eu^{2+} ground state could be observed in the K band. They are caused by effects of cross-relaxation between Eu^{2+}, and the recombining electron and hole centres, respectively [16]. A spin flip in the Eu^{2+} system leads to a spin flip in one of the recombining centres and thus to an enhanced RL which can be seen in the RL-EPR spectrum. The cross-relaxation effect has only been observed for the RL-EPR measurements in the K band, but not for those in the W band. The cross-relaxation probability depends on the overlap integral of the EPR lines of Eu^{2+} and the electron (F) and/or the hole (V_K) centre, a requirement of energy conservation between the spin systems [16]. This overlap is decreased in higher magnetic fields and thus the cross-relaxation effect could not be observed any longer.

The W-band RL-EPR measurements yielded a g-value for an orientation of the magnetic field parallel to the crystal axis c of $g_c = 1.986$ (3371 mT for 93.7 GHz) which is identical to the value determined by conventional X-band EPR investigations [4]. For an orientation parallel to the a-axis we could resolve the g-values for the two different F centres. We obtained $g_a = 1.976$ (F_I, 3387 mT for 93.7 GHz) and $g_a = 1.962$ (F_{II}, 3412 mT for 93.7 GHz). The value of $g_a = 1.968$ obtained by the conventional EPR measurements [4] is almost the average between the two W-band values, i.e. the two g-values could not be resolved in the X band.

The absorption spectra of $BaBr_2$ show that the main defects observed after low-temperature irradiation are F and V_K centres. There is a strong correlation between the thermal decay of the V_K centres after annealing to 135 K and the glow peak at 106 K. The TL spectrum, recorded in the glow peak, shows predominantly the band at around 460 nm which is due to the luminescent F–V_K recombination. We suppose that the 0.27 eV activation energy of this glow peak corresponds to the diffusion energy of the V_K centres. A similar situation occurs in KI irradiated at 80 K: the V_K diffusion energy of 0.273 eV [17] agrees quite well with the 0.27 eV activation energy of the 105 K glow peak [18].

A structure-sensitive analysis of the defects leading to the 282 and 315 nm luminescence bands by means of RL-EPR or x-ray luminescence-detected EPR (XL-EPR) has not been

possible. Since the RL-EPR/XL-EPR experiments had to be performed at 1.5 K (better signal-to-noise ratio), only the 282 nm luminescence band, and not the 315 nm band which appears above about 40 K, could be investigated. The reason that we did not find any EPR in the 282 nm band could be either too large fine-structure splitting (assuming a self-trapped exciton (STE) triplet state with $S = 1$) or too fast relaxation times. However, in analogy to alkali halides (see e.g. [19] and references therein) two different models may be discussed. The first one suggests that the two luminescence bands are due to recombinations of STEs having two different configurations. The small Stokes shift between the first excitonic absorption band of $BaBr_2$ at 164 nm (7.55 eV) [20] and the STE luminescences at 282 and 315 nm indicates that no large relaxation of the exciton occurs after its creation. In alkali halides the Stokes shift characterizes the electron–hole separation; a larger shift means higher separation and vice versa. Thus, these bands could be due to STEs which have a configuration of V_K + e type, i.e. a Br_2^{2-} molecule with an electron in an excited state. There are two different configurations for the V_K centre possible in $BaBr_2$: 'in-plane' and 'out-of-plane' [7]. The second possibility is that these bands are due to singlet and triplet state recombinations of only one STE type. In each of the above-mentioned cases a potential barrier determines the thermally activated transformation from one exciton configuration into another or from a singlet to a triplet state configuration, respectively.

The intensity decrease of the 282 nm band upon warming can be explained by a thermally activated transformation of one radiative exciton configuration into another non-radiative one, which competes with the 282 nm radiative transition. The intensity behaviour can be described by [21]

$$I = \frac{I_0}{1 + A\exp(-E/kT)} \tag{2}$$

where E is the potential barrier for the transformation and the constant $A = \tau_{rad}/\tau_{non}$ is the ratio of the radiative lifetime τ_{rad} to the non-radiative lifetime τ_{non}. Analysing the experimental data results in $E = 0.04 \pm 0.01$ eV for the potential barrier. Due to the lack of experimental data we determined the constant A as being approximately $A = 10^5$–10^7 and varied only the energy E.

In Eu-doped $BaBr_2$, the STE recombination energy is transferred to Eu^{2+} which has a broad absorption band in the ultraviolet spectral range. Surprisingly, no oxygen-related luminescence band could be observed in oxygen-doped $BaBr_2$.

The recombination processes leading to the 31 K TL peak could not be identified. The nature of the 282 nm band, which shows up in the corresponding TSL spectrum, is not clarified (see above); nor could a clear change be observed in the absorption spectrum after thermal annealing. Although the glow peak has an activation energy of 0.05 eV which is very close to the average activation energy for H centre diffusion in alkali halides [19], the assignment of this peak to H centre diffusion and recombination of F centres is very questionable. Even after prolonged x-ray irradiation at low temperatures we did not find any EPR resonances which can be attributed to H-type (interstitial bromine atom) hole centres. Probably other defects such as I centres (interstitial bromide) could also be involved in the recombination processes (see e.g. KCl and KBr) [22, 23].

5. Conclusions

The RL-EPR of $BaBr_2$ showed that the low-energy RL band at about 460 nm is due to F–V_K centre recombinations. The high-energy bands at 282 and 315 nm are probably due to STE recombinations. The observed Eu^{2+} resonances in the RL-EPR spectrum of $BaBr_2$:Eu^{2+} could

be explained by effects of cross-relaxation between Eu^{2+} and the recombining F and/or V_K centres. The RL-EPR angular dependence in the W band confirmed that both types of F centre are created after x-irradiation at low temperatures. The optical absorption and TL show that the V_K centres decay at about 106 K.

Acknowledgment

The authors would like to thank the Deutsche Forschungsgemeinschaft for financial support.

References

[1] Edgar A, Spaeth J-M, Schweizer S, Assmann S, Newman P J and Macfarlane D R 1999 *Appl. Phys. Lett.* **75** 2386
[2] Edgar A, Secu M, Williams G V M, Schweizer S and Spaeth J-M 2001 *J. Phys.: Condens. Matter* **13** 6259
[3] Secu M, Schweizer S, Spaeth J-M, Edgar A, Williams G V M and Rieser U 2003 *J. Phys.: Condens. Matter* **15** 1097–108
[4] Grujic D, Houlier B, Yuste M, Taurel L and Chapelle J P 1970 *C. R. Acad. Sci., Paris* **270** 1355
[5] Houlier B, Yuste M, Chapelle J P and Taurel L 1972 *Phys. Status Solidi* b **51** 881
[6] Houlier B 1977 *J. Phys. C: Solid State Phys.* **10** 1419
[7] Moreno M 1975 *Solid State Commun.* **16** 1239
[8] Moreno M 1977 *Cryst. Latt. Defects* **7** 27
[9] Schweizer S, Rogulis U and Spaeth J-M 1998 *Radiat. Meas.* **29** 283
[10] Rogulis U, Schweizer S and Spaeth J-M 1999 *Radiat. Eff. Defects Solids* **149** 69
[11] Monberg E and Ebisuzaki Y 1974 *J. Cryst. Growth* **21** 307
[12] Kirsh Y 1972 *Phys. Status Solidi* a **129** 15
[13] Iwase N, Tadaki S, Hidaka S and Koshino N 1994 *J. Lumin.* **60/61** 618
[14] Brackett E B, Brackett T E and Sass R L 1963 *J. Phys. Chem.* **67** 2132
[15] Schweizer S, Corradi G, Edgar A and Spaeth J-M 2001 *J. Phys.: Condens. Matter* **13** 2331
[16] Koschnick F-K, Spaeth J-M and Eachus R S 1992 *J. Phys.: Condens. Matter* **4** 8919
[17] Keller F J and Murray R B 1966 *Phys. Rev.* **150** 670
[18] Matei L, Serban T, Secu M and Beica T 1997 *J. Lumin.* **72–74** 691
[19] Song K S and Williams R T 1993 *Self-Trapped Excitons (Springer Series in Solid-State Sciences vol 105)* (Springer: Berlin)
[20] Nicklaus E 1979 *Phys. Status Solidi* a **53** 217
[21] Williams R T and Song K S 1990 *J. Phys. Chem. Solids* **51** 679
[22] Aboltin D E, Grabovskis V J, Kangro A R, Luschik Ch B, O'Konnel-Bronin A A, Vitol I K and Zirap V E 1978 *Phys. Status Solidi* a **47** 667
[23] Alvarez Rivas J L 1980 *J. Physique Coll.* **41** C6 353